A novel U-bent plastic optical fibre local surface plasmon resonance sensor based on a graphene and silver nanoparticle hybrid structure

2017 J. Phys. D: Appl. Phys. 50 165105

(http://iopscience.iop.org/0022-3727/50/16/165105)

IOP Publishing Journal of Physics D: Applied Physics

J. Phys. D: Appl. Phys. **50** (2017) 165105 (10pp) https://doi.org/10.1088/1361-6463/aa628c

A novel U-bent plastic optical fibre local surface plasmon resonance sensor based on a graphene and silver nanoparticle hybrid structure

Shouzhen Jiang[1,2,5], Zhe Li[1,5], Chao Zhang[1,2], Saisai Gao[1], Zhen Li[1], Hengwei Qiu[3], Chonghui Li[1], Cheng Yang[1,2], Mei Liu[1,2] and Yanjun Liu[4]

[1] School of Physics and Electronics, Shandong Normal University, Jinan 250014, People's Republic of China
[2] Institute of Materials and Clean Energy, Shandong Normal University, Jinan 250014, People's Republic of China
[3] Electronic Materials Research Laboratory Key Laboratory of the Ministry of Education, International Center for Dielectric Research, Xi'an Jiaotong University, Xi'an, Shanxi 710049, People's Republic of China
[4] Department of Electrical and Electronic Engineering, Southern University of Science and Technology, Shenzhen 518055, People's Republic of China

E-mail: jiang_sz@126.com (S Jiang)

Received 11 January 2017, revised 14 February 2017
Accepted for publication 23 February 2017
Published 24 March 2017

Abstract

In this work, we have presented a novel local surface plasmon resonance (LSPR) sensor based on the U-bent plastic optical fibre (U-POF). Firstly, a layer of discontinuous silver (Ag) thin film was deposited on the U-POF and then the Ag film was covered by a layer of cladding synthesized by polyvinyl alcohol (PVA), graphene and silver nanoparticles forming the PVA/G/AgNPs@Ag film. The normalized transmittance spectrum of the LSPR sensor have been collected in a range of the refractive index (RI) from 1.330 to 1.3657 in ethanol solution, and 700.3 nm/RIU sensitivity of the developed LSPR sensor has been demonstrated. By experiments, we demonstrated that the graphene could improve the sensitivity of the LSPR sensor and delay the oxidation process of the AgNPs effectively to keep the stability of the LSPR sensor. The LSPR sensor also exhibited good sensitivity and linearity in the detection of glucose solutions. This work shows that the developed LSPR sensor may have promising applications in biosensing.

Keywords: local surface plasmon resonance, plastic optical fibre, graphene, sensor, sensitivity, stability

(Some figures may appear in colour only in the online journal)

1. Introduction

In recent years, the local surface plasmon resonance (LSPR) technique has received a lot of attention due to its applications in the sensing of various physical, chemical and biological parameters [1–4]. The deployment of optical fibres as LSPR devices has achieved an outstanding position due to its advantages, such as high sensitivity to the refractive index (RI) change and ease of fabrication, modification and control. Up to now, a great effort has been made to improve the performance of the optical fibre LSPR sensors [5, 8]. LSPR is similar to the well-known surface plasmon resonance (SPR) phenomenon, where the environmental changes at the interfaces between

[5] These authors contributed equally.

media and metals can be traced by the changes of metal LSPR characteristics, because the localized electromagnetic field around metal surfaces is very sensitive to environmental RI [9, 10]. In general, for optical fibre LSPR sensors, an evanescent field is needed to generate surface plasmon waves (SPW) at the interface of metal nanoparticles and the surrounding medium [11]. The typically used metals are gold and silver [12–14]. Based on this, many different structures of optical fibre have been made to study, such as partially unclad [15], side-polished [16], tapered optical fibres [17, 18], photonic crystal fibre [19], D-shaped optical fibre [20], fibre-grating SPR sensors [21] and U-bent optical fibre [22, 23], and it has been proved that the U-bent optical fibre possesses higher sensitivity, because of the variation of the angle of incidence [22]. So far, optical fibre SPR or LSPR sensors are typically made from all silica fibres, however these fibres remain at a high cost and are fragile. Recently, plastic optical fibre (POF) has received more attention than the conventional silica fibres due to their ease in machinability, handling and low cost; therefore POF gets a lot of production and applications [24, 25].

Research has found that the performance of LSPR sensors can be tuned by the properties of the capping material, surface charge and interparticle interaction, more efficiently than the size of the particle [26]. Therefore, investigation for the capping material, the surface charge and interparticle interaction is significant for the LSPR sensors.

Graphene, a single layer of the sp^2 carbon network arranged in a perfect honeycomb lattice, is one of the most extensively studied 2D nanomaterials to date since its first discovery in 2004 [27–29]. The charge carrier mobility of graphene is reported to be as high as 10^6 cm^2 V^{-1} s^{-1} [30]. When graphene layers are deposited on metallic thin films or metallic nanoparticles (e.g. Au or Ag), strong coupling can be induced at the metallic/graphene interface due to the effective charge transfer, generating a large electric field enhancement at the nanointerface [31–39]. Graphene has relatively large surface area (~2630 m^2 g^{-1}), thus allowing it to have better surface contact with the analyte and absorb more molecules [40]. Taking these advantages of graphene, the LSPR sensors with improved sensitivity can be offered, but few groups combined the optical fibre LSPR with the graphene in the experiment. What is more, the stability is also important for the LSPR sensor; graphene on the surface of metal can prevent the oxidation of the metallic thin film and keep the stability of the sensors effectively.

In this paper, combining the advantages of the U-bent optical fibre, POF and graphene, we fabricated a novel LSPR sensor based on the U-bent plastic optical fibre (U-POF) with PVA, AgNPs, graphene and a layer of discontinuous Ag film (PVA/G/AgNPs@Ag film U-POF). Firstly, a new and simple method was utilized to fabricate the U-POF and then a layer of thin discontinuous silver film was deposited on it. PVA is a proven capping agent and matrix in the synthesis of different nanoparticles [41, 42], therefore the hybrid structure of PVA, AgNPs and graphene was coated on the surface of the Ag film. We demonstrated that the graphene could improve the sensitivity of the LSPR sensor and delay the oxidation process of the AgNPs effectively to keep the stability of the LSPR sensor. The developed LSPR sensor exhibited good sensitivity (700.3 nm/RIU), stability and linearity in the detection of the ethanol and glucose solutions. The work shows that the developed LSPR sensor may have promising applications in biosensing.

2. Experimental

2.1. Fabrication of U-POF

Figure 1 schematically illustrates the process for the synthesis of PVA/G/AgNPs@Ag film U-POF. As is shown in figure 1, the cladding of the 30 cm long POF (diameter = 1 mm) was stripped, the bare part is 2 cm long, and the surface cladding of the bare POF was removed by acetone. Then we fixed the POF on the iron stand and the U-POF should keep 1 cm distant from the outer flame. The U-POF was moved right and left rapidly for 10 cycles (about 3 s) over the flame, then the U-POF was cooled to room temperature and rinsed by deionized water. Because both arms of the U-POF have been fixed on the iron stand, the inner diameter (5 mm) of the U-POF remains constant, and the shape of the U-POF can be controlled and repeated easily.

2.2. Synthesis of PVA-AgNPs composites

Making use of the reducibility of the PVA to the $AgNO_3$, the AgNPs are directly synthesized in the PVA matrix in few steps. Firstly, PVA (0.5 g) was dissolved in hot deionized water (25 ml) under magnetic stirring in order to obtain a colourless transparent PVA solution. Then $AgNO_3$ solution (4 mM, 125 ml) was added into the aqueous solution of PVA, the mixed solution underwent constant magnetic stirring and heating under 60 °C –70 °C for 2 h, the colour of the solution deepened gradually from an achromatic colour in the beginning to a faint yellowish equilibrium colour, then the PVA-AgNPs composites were cooled at 20 °C–24 °C.

2.3. Synthesis of the PVA/G/AgNPs@Ag film U-POF

The 3 nm, 5 nm and 10 nm thick Ag thin film was deposited on the prepared U-POF respectively via thermal evaporation. Firstly, 0.5 ml of 1 mg ml^{-1} graphene solution was mixed with 2.5 ml of PVA-AgNPs solution and then it was fully stirred to form the PVA/G/AgNPs solution. Then the PVA/G/AgNPs solution was coated on the U-POF by dip-coating, as shown in figure 1, and it was finally dried under nitrogen atmosphere.

2.4. Optical set-up and characterization instrument

The experimental set-up contains four portions, as shown in figure 2; in the order from left to right is the light source, U-bent fibre, spectrometer (PG2000, Ideaoptics Instruments) and the PC. The light source provides the steady light intensity and the range of the light source wavelength is from 380 nm to 780 nm. One end of the U-bent optical fibre was coupled to the light source and another end was coupled to

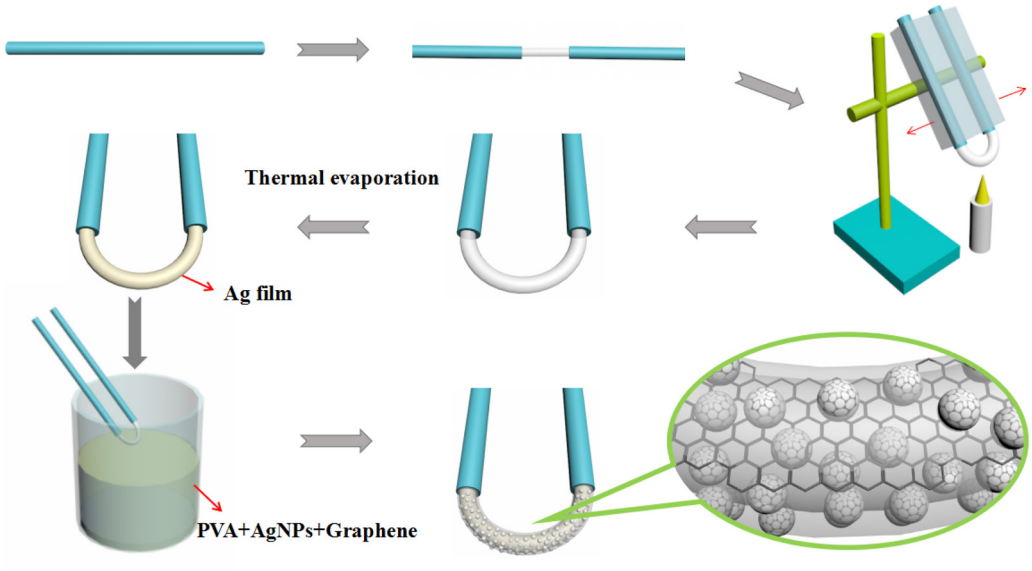

Figure 1. The schematic representation of the preparation procedure of the PVA/G/AgNPs@Ag film U-POF.

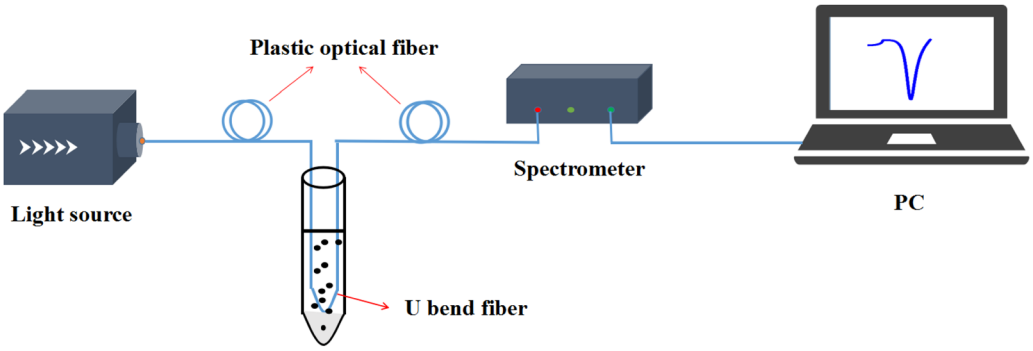

Figure 2. The schematic diagram for the experimental set-up used in the U-bent optical fibre LSPR sensor.

the spectrometer using an optical fibre patch cord. The intensity of light coupled into the fibre changed when the U-POF was immersed in ethanol solution with a different RI. The output light was collected and full transmittance spectra were recorded by a spectrometer. At last, Morpho software installed on the computer was used to process the data recorded by the spectrometer.

The surface morphology of the LSPR sensor was characterized by scanning an electron microscope (SEM, Zeiss Gemini Ultra-55) and an atomic force microscope (AFM, Park XE-100) in the noncontact mode. The transmittance electron microscopy (TEM) is carried out by a TEM system (Hitachi H-800). The Raman spectrum of graphene was carried out with a Horiba HR Evolution 800 Raman spectrometer with laser wavelength at 532 nm. The spectra were collected under the same conditions (integration time: 4 s), the excitation laser spot was about 1 μm, and the effective power of the laser source was kept at 50 mW.

3. Results and discussion

Figure 3(a) shows the SEM image of the bare U-POF. As we can see, the surface of the U-POF is smooth, it is conducive to the adsorption of metal particles during the process of the thermal evaporation and the good quality of the U-POF provides the possibility for the following experiment. Figures 3(b) and (c) show the photos of the Ag film/U-POF and PVA/G/AgNPs@Ag film U-POF, respectively; by contrast, we can find that the colour of the cladding turned from silvery to dark yellow with the addition of the PVA/graphene/AgNPs. As we can see in the pictures, the inner diameter of the U-POF is about 5 mm and the length of the coating is about 2 cm.

In order to select the optimal thickness of the Ag film, we detected the normalized transmittance spectra of the U-POF deposited by 3, 5, 6, 7 and 10 nm thick Ag film in the ethanol solution with different RI from 1.330 to 1.3657, respectively. As shown in figures 4(a)–(e), we found that the U-POF with 5 nm thick Ag film presents the relatively good LSPR dip, and there is an obvious red shift of the resonance wavelength with the increase of the RI in figure 4(b), which in figures 4(a) and (e) is invisible. The red shift in figures 4(c) or (d) is less than that in figure 4(b). In fact, to reduce random errors in the RI sensing, we have adopted the weighted centroid algorithm to ensure the dip center wavelength, this method can improve the measurement accuracy effectively. In order to compare the sensitivity of U-POFs with the different thickness of Ag film, we give the wavelength shift at the RI from 1.3330 to 1.3657 as a function of the thickness of the Ag film in figure 4(f). As

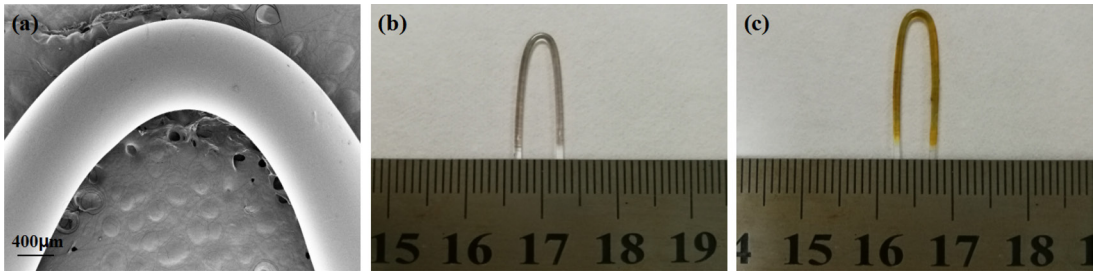

Figure 3. (a) SEM image of bare U-POF. (b) and (c) Photos of the Ag film/U-POF and PVA/G/AgNPs@Ag film U-POF respectively.

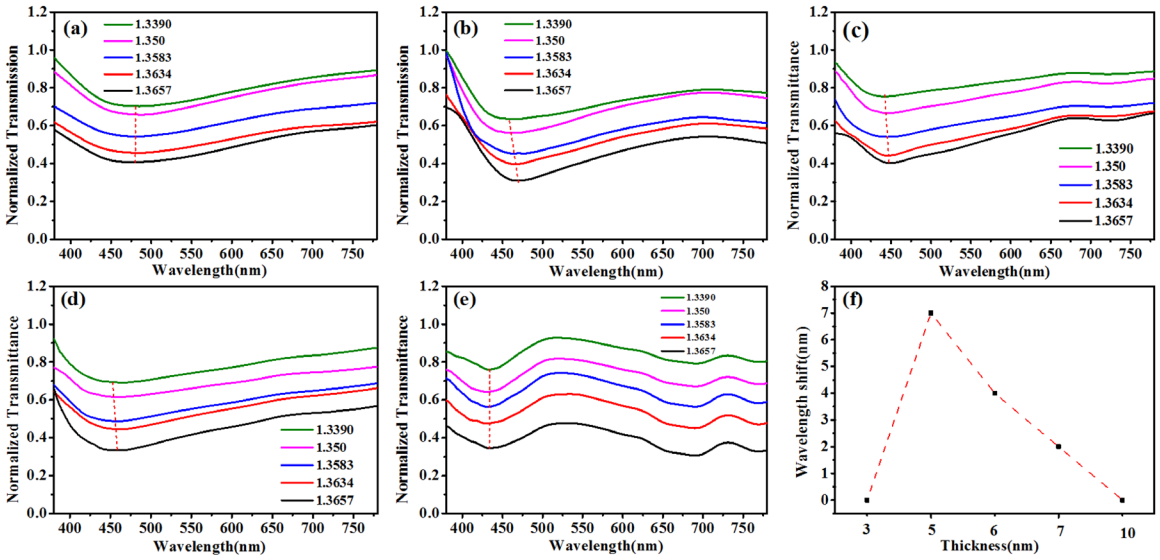

Figure 4. (a)–(e) Normalized transmittance spectra of U-POF deposited by 3, 5, 6, 7 and 10 nm thick Ag film in the ethanol solution with a different RI from 1.3330 to 1.3657, respectively. (f) Wavelength shift at the RI from 1.3330 to 1.3657 as a function of the thickness of the Ag film.

shown in the figure, we can find that the resonance wavelength shift is almost 0 nm when the thickness of the Ag film is 3 nm or 10 nm. From 5 nm to 7 nm, the wavelength shift decreases gradually, the 5 nm thick Ag film shows wider wavelength shift. It means that the U-POF with 5 nm thick Ag film possesses high sensitivity relatively. Therefore, we can ensure that the optimal thickness of the Ag film is 5 nm in our work.

After that, we detected the surface morphology of U-POF with 5 nm thick Ag film as shown in figures 5(a) and (b), we can find that the Ag film is not continuous on the surface of U-POF and the AgNPs possess good uniformity, and figure 5(c) is the AFM image of the Ag film with the thickness of 5 nm on the U-POF. We have scratched a line on the Ag film along the longitudinal direction of POF using a pinpoint to form the brown line. The tip of the AFM scans along the transverse direction of the POF in a small range of 50 μm and the curve of the inset shows the thickness of the Ag film.

Although the U-POF with 5 nm Ag film shows the relatively good effect of the LSPR, it still needs to be improved. Therefore, we chose to tune the LSPR by adding a layer of capping material synthesized by PVA, graphene and AgNPs on the surface of the 5 nm thick Ag film. Figures 6(a) and (b) show the SEM images of the PVA/G/AgNPs@Ag film U-POF; as we can see in the figure 6(b), the AgNPs distribute uniformly in the coating. Figure 6(c) shows the TEM image of the AgNPs reduced by PVA. The diameter of the AgNPs is about 15 nm, meanwhile, we detected the graphene on the surface of the PVA/G/AgNPs@Ag film U-POF by the Raman spectrometer; as shown in figure 6(d), the D peak and G peak, which are the characteristic peaks of graphene, can be detected easily. Therefore, we can prove that the graphene exists in the coating.

To evaluate the performance of the LSPR sensor, we detected the normalized transmittance spectra of PVA/AgNPs U-POF, PVA/AgNPs@Ag film U-POF and PVA/G/AgNPs@Ag film U-POF in the ethanol solution with different RI from 1.3330 to 1.3657, respectively. As shown in figures 7(a)–(c), overall, it can be seen that the red shift of the LSPR band positions took place and the transmission peak intensities reduced gradually with the RI increasing. By comparing figure 7(a) with (b), we found that the PVA/AgNPs@Ag film U-POF possesses a deeper LSPR dip than PVA/AgNPs U-POF, and by the red dash line we know that the former red shift of LSPR band positions is more than the latter. This indicates that the Ag film plays an essential role in the sensing mechanism, and it could improve the sensitivity of the LSPR sensors. Then, with the addition of graphene, we found that in figure 7(c) the transmittance dropped obviously compared with that in the figure 7(b) overall. Meanwhile, with the aid of red dash line, we found that the red shift of resonance wavelength got larger. Then the

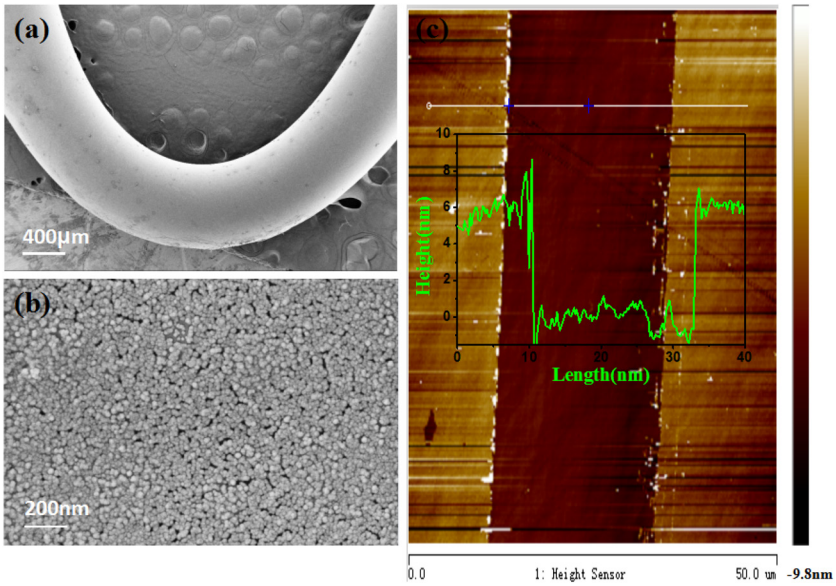

Figure 5. (a) and (b) SEM images of the U-POF with 5 nm thick Ag film under different magnification. (c) The AFM image of the Ag film on the U-POF. The inset shows the thickness curve of the Ag film.

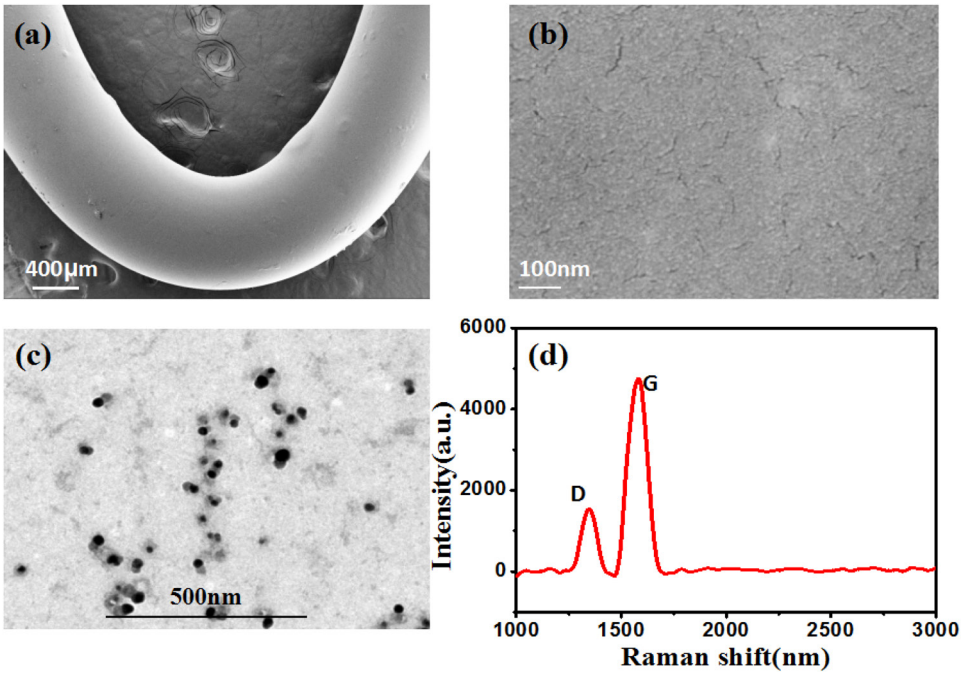

Figure 6. (a) and (b) SEM images of the PVA/G/AgNPs@Ag film U-POF under different magnification. (c) The TEM image of the AgNPs in the coating. (d) The Raman spectra of the graphene in the coating.

transmittance at 461 nm, 459 nm and 484 nm was chosen to plot the LSPR response to the RI of ethanol solution; as shown in figures 7(d)–(f), the sensitivity and coefficient of determination (R^2) of the fit calibration curve for the three kinds of U-POF are 9.46 TU/RIU ($R^2 = 0.898$), 11.34 TU/RIU ($R^2 = 0.917$) and 15.33 TU/RIU ($R^2 = 0.988$), respectively. Obviously, both the sensitivity and the linearity of the PVA/G/AgNPs@Ag film U-POF are higher in figure 7(f), the good sensitivity and linear relationship of the PVA/G/AgNPs@Ag film U-POF between transmittance and RI can be ascribed to graphene, which has a relatively high surface-to-volume ratio, thus allowing it to have a better surface contact with the analyte and absorb more molecules. The tunable RI of the grapheme, with the concentration increase of the ethanol solution, leads to a more significant absorbance variation. The sensitive RI change of the sensing area with graphene is introduced by the molecular enrichment properties of graphene.

In order to compare the sensitivities of the three kinds of U-POFs more visually, we take the wavelength shift changes as a function of RI of ethanol and the linear relationship was shown in figure 8(a). As we can see, it is obvious that the PVA/G/AgNPs@Ag film U-POF possesses a higher sensitivity, which is 700.3 nm/RIU. To compare the sensing performance of the developed LSPR sensor, the detecting

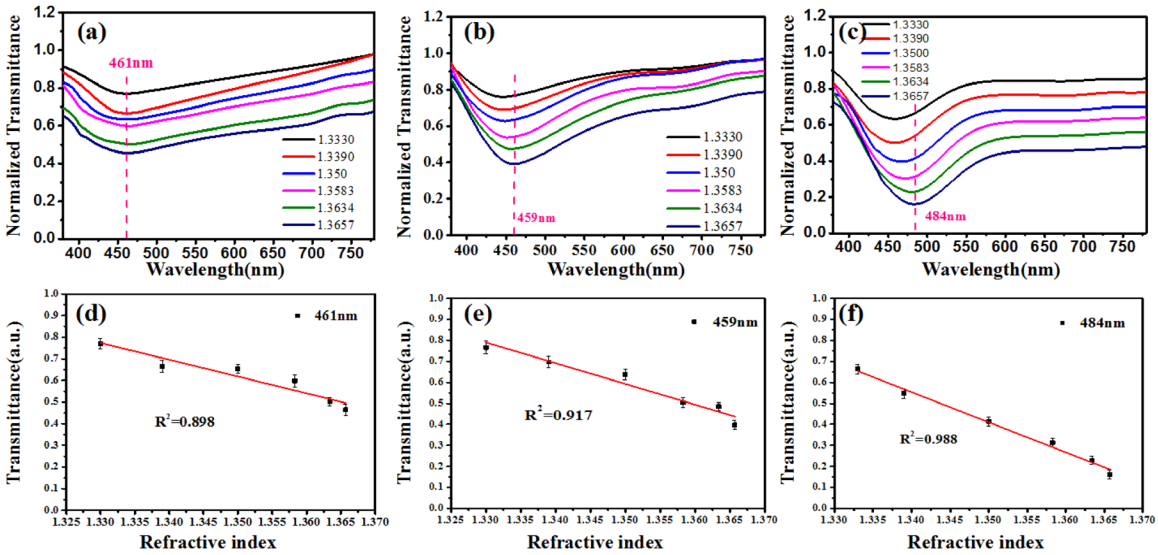

Figure 7. (a)–(c) Normalized transmittance spectra of the PVA/AgNPs U-POF, PVA/AgNPs@Ag film U-POF and PVA/G/AgNPs@Ag film U-POF in ethanol solution with RI from 1.3330 to 1.3657 respectively. (d)–(f) Transmission at 461 nm, 459 nm and 484 nm as a function of the RI corresponding (a)–(c), respectively.

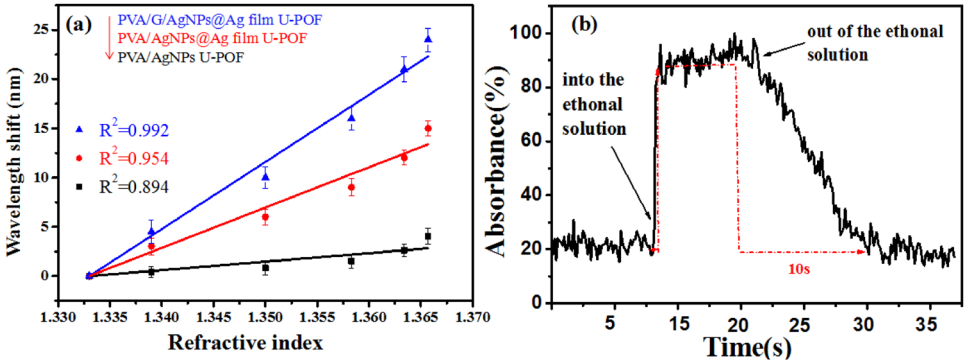

Figure 8. (a) Wavelength shift of PVA/AgNPs U-POF, PVA/AgNPs@Ag film U-POF and PVA/G/AgNPs@Ag film U-POF as a function of RI, respectively. (b) Typical response-recovery characteristic curves of the PVA/G/AgNPs@Ag film U-POF at 484 nm in the ethanol solution with the RI of 1.3657.

sensitivity was compared with that of other optical fibre LSPR sensors utilizing different approaches reported in the literature in table 1. By the contrast data in table 1, our sensor presents higher sensitivity. The main reason we concluded this is that graphene possesses good biocompatibility, which could absorb more molecules, and the strong coupling can be induced at the AgNPs/graphene interface due to the effective charge transfer, and this generates a large electric field enhancement at the nanointerface. These led to a good sensitivity of the LSPR sensor. The R^2 of the fit calibration curves for the three kinds of U-POFs are 0.894, 0.954 and 0.992, respectively. It indicates that the PVA/G/AgNPs@Ag film U-POF also has a good linear relationship between the wavelength shift and the RI. Figure 8(b) shows the typical response-recovery characteristic curves of the PVA/G/AgNPs@Ag film U-POF at 484 nm in the ethanol solution with the RI of 1.3657. As shown in this figure, when the PVA/G/AgNPs@Ag film U-POF was placed into the ethanol solution, the response is fast and the absorbance rises to 90% immediately. The fast response may be due to ethanol molecule enrichment and the high surface-to-volume ratio of graphene. Then we take out the U-POF and it takes 10 s to recover. The reason may be that the graphene possesses high absorbability for the ethanol molecules and the ethanol molecules cannot volatilize immediately.

Table 1. Comparison of the sensitivities between some optical fibre LSPR sensors.

Sensor type	Material	Sensitivity (nm/RIU)	Reference
Tapered fibre	AuNPs	66.7	[5]
End reflection	AgNPs	67.6	[43]
End reflection	AuNPs	196	[2]
D-shape fibre	Au nanostars	580	[18]
U-bent fibre	AgNPs and graphene	700.3	Present study

In order to evaluate how the U-bent inner diameter affects the performance of the sensor, the further work has been expanded. We have fabricated two other PVA/G/AgNPs@Ag film U-POFs with different U-bent inner diameters ($D = 7$ mm and 9 mm) in the same way, and then we detected

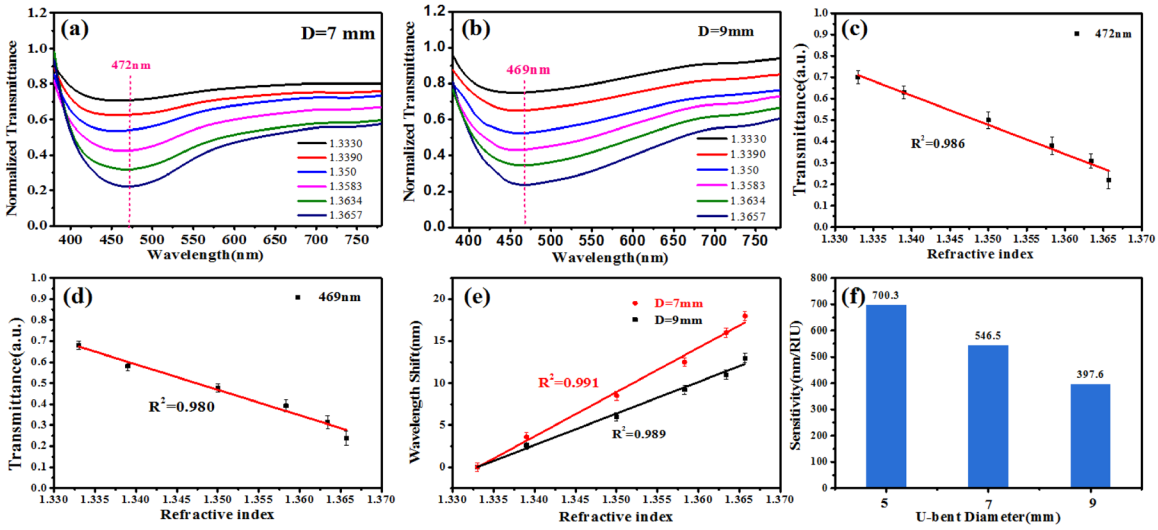

Figure 9. (a) and (b) Normalized transmittance spectra of the PVA/G/AgNPs@Ag film U-POF having different U-bent inner diameters ($D = 7$ mm and 9 mm) in ethanol solution with RI from 1.3330 to 1.3657 respectively. (c) and (d) Transmission at 472 nm and 469 nm as a function of the RI corresponding (a) and (b), respectively. (e) Wavelength shift of PVA/G/AgNPs@Ag film U-POF with 7 mm and 9 mm U-bent inner diameters as a function of RI, respectively. (f) Sensitivity histogram of the PVA/G/AgNPs@Ag film U-POF with 5 mm, 7 mm and 9 mm U-bent inner diameters.

the normalized transmittance spectra of the two PVA/G/AgNPs@Ag film U-POFs in the ethanol solution with a different RI from 1.3330 to 1.3657, respectively, as shown in figures 9(a) and (b). By convention, we detected the transmittance at 472 nm and 469 nm to plot the LSPR response to the RI of the ethanol solution; as shown in figures 9(c) and (d), the sensitivity and coefficient of determination (R^2) of the fit calibration curve for the two PVA/G/AgNPs@Ag film U-POFs are 14.67 TU/RIU ($R^2 = 0.986$), 13.54 TU/RIU ($R^2 = 0.980$), respectively. With the decrease of the U-bent inner diameter, the sensitivity and R^2 increase slightly. These results are in good agreement with reported literature [6, 44]. Previous research found that the sensitivity cannot be increased infinitely by decreasing the U-bend inner diameter; an optimum U-bending inner diameter may be found [45]. The existence of the optimum diameter can be attributed to the cross coupling of the power between the two arms of the U-bent probe [45]. In our work, we could not fabricate the U-bent probe with the U-bent inner diameters below 5 mm in spite of our best efforts. Then we took the wavelength shift changes as a function of the RI of ethanol, and the linear relationship was shown in figure 9(e). As we can see, with the increase of the U-bent inner diameter, the red shift reduces from 18 nm to 13 nm. Finally, to intuitively observe the difference of sensitivity among the three PVA/G/AgNPs@Ag film U-POFs with different U-bent inner diameters, we give the sensitivity histogram of the PVA/G/AgNPs@Ag film U-POF with 5 mm, 7 mm and 9 mm U-bent inner diameters in the figure 9(f). As shown in the figure, with the increase of the U-bent inner diameters from 5 mm to 9 mm, the sensitivity of the LSPR sensor decreases from 700.3 nm/RIU to 397.6 nm/RIU. This trend indicates that the sensitivity of the LSPR sensor may increase with smaller U-bent inner diameters. However, the optimum diameter could not be observed up as a result of the limitation of our experimental equipment and the smallest U-bent inner diameter we can fabricate is 5 mm. Therefore the 5 mm U-bent inner diameter is the optimum in our work.

Besides the sensitivity, the stability is an important parameter for estimating sensing performance. Six cycles of the normalized transmittance at the RI of 1.350 were performed under the same conditions to investigate the reproducibility of this PVA/G/AgNPs@Ag film U-POF sensor. As shown in figure 10(a), the spectra almost stay constant and the good reproducibility of this sensor can be confirmed after the six cycles. Figure 10(b) shows the absorbance distribution at 468 nm and the wavelength shift curve of the PVA/G/AgNPs@Ag film U-POF sensor immersed in ethanol solution with the RI of 1.350 for a period of 10 h. As we can see, in the first 5 h, the absorbance and wavelength shift curve remain nearly constant, then start from the fifth hour, both of them gradually decrease and tend to be stable finally. The main reason for this phenomenon may be that the PVA can dissolve a little in the ethanol solution when they are immersed in it for a certain period of time. This is something we should pay attention to. In general, the LSPR sensor shows a relatively good stability. What is more, the stability of materials can also determine the stability of the LSPR sensor. It is well known that AgNPs are easy to oxidize in the laboratory condition, therefore the oxidation prevention of the sensor is an important work. To evaluate the antioxidant effect of the graphene for our LSPR sensor, we contrast the normalized transmittance spectra of the PVA/AgNPs@Ag film U-POF with the PVA/G/AgNPs@Ag film U-POF in the ethanol solution with the RI of 1.350 on the first and fifteenth days in the laboratory condition, respectively. As shown in figures 10(c) and (d), compared with the first day, the PVA/AgNPs@Ag film U-POF has almost no LSPR dip on the fifteenth day, while the PVA/G/AgNPs@Ag film U-POF still has a deep LSPR dip relatively. This phenomenon indicates that with the addition of graphene, the antioxidant ability of the PVA/G/AgNPs@Ag film U-POF has risen

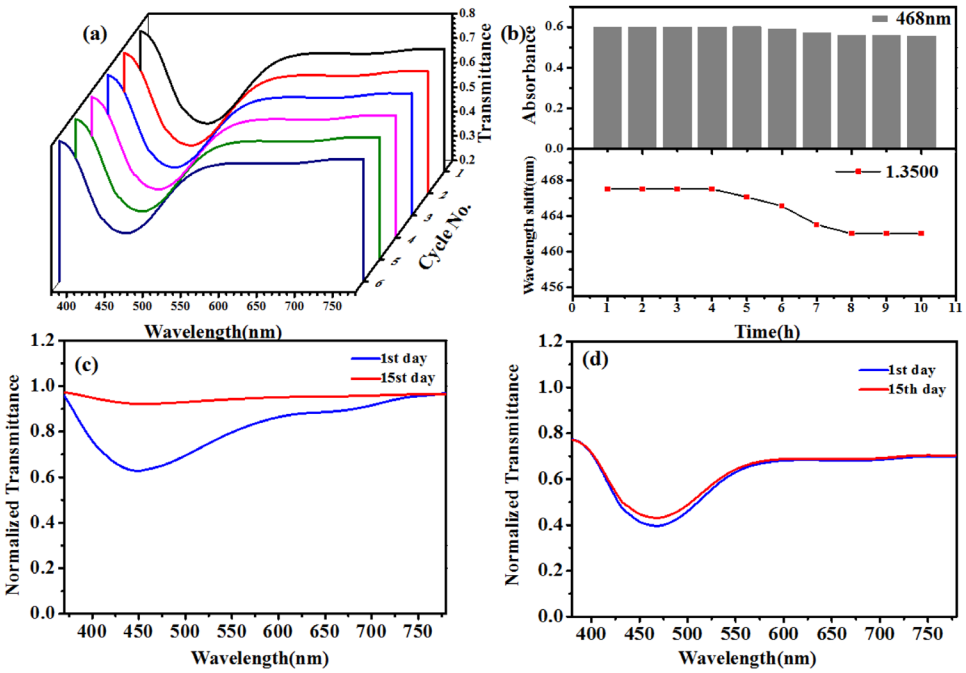

Figure 10. (a) Normalized transmittance spectra at the RI of 1.350 during six cycles obtained from the PVA/G/AgNPs@Ag film U-POF sensor. (b) Absorbance distribution at 468 nm and the wavelength shift curve of the PVA/G/AgNPs@Ag film U-POF sensor immersed in ethanol solution with the RI of 1.350 for a period of 10 h. (c) and (d) Normalized transmittance spectra of the PVA/AgNPs@Ag film U-POF and the PVA/G/AgNPs@Ag film U-POF in the ethanol solution with the RI of 1.350 on the first day and the fifteenth day in the laboratory condition, respectively.

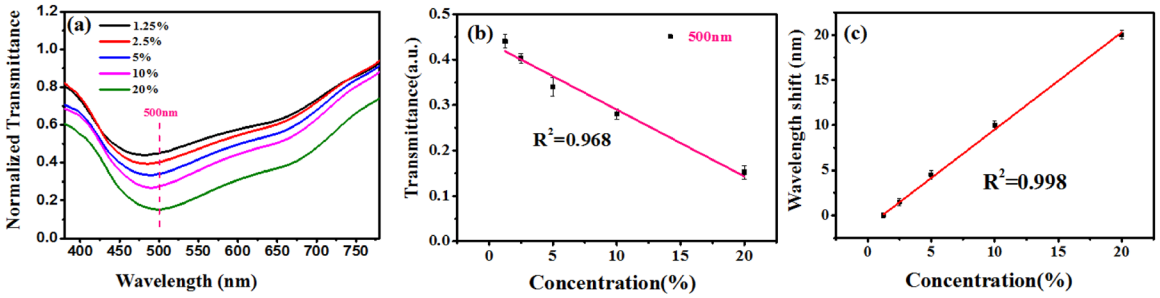

Figure 11. (a) Normalized transmittance spectra of PVA/G/AgNPs@Ag film U-POF in the glucose solution with different concentrations. (b) Transmittance at 500 nm as a function of the RI. (c) Wavelength shift as a function of the concentration in the glucose solution.

notably, and stability of the LSPR sensor can be ensured. Therefore the graphene plays an important role in the stability of the developed LSPR sensor.

What is more, to investigate the feasibility of the PVA/G/AgNPs@Ag film U-POF in practical application, the glucose solution with the concentration of from 1.25% to 20% was detected. Glucose plays an important role in the field of biology; it is the source of energy and metabolism of living cells and is one of the most widely distributed and most important monosaccharide in nature. As shown in figure 11(a), it presents a series of transmittance spectra of the LSPR sensors incubated with different concentrations of glucose solution. Similarly, it can be seen that the red shift of the LSPR band positions took place and the transmittance peak intensities reduced gradually with the RI increasing too. The transmittance at 500 nm as a function of the RI shift is given in figure 11(b). It also exhibited a good linear relationship between the transmittance and concentration ($R^2 = 0.968$). Figure 11(c) shows the linear relationship between the wavelength shift and concentration. As we can see, the red shift of LSPR band positions is about 20 nm, the R^2 of the fit calibration curve is 0.998 and the developed LSPR sensor also shows a relatively good sensitivity and linearity in the detection of glucose solutions.

4. Conclusions

In this work, we have fabricated a LSPR sensor with the sensitivity of 700.3 nm/RIU based on the PVA/AgNPs@Ag film U-POF. Through comparative analysis, we demonstrated that the graphene could improve the sensitivity of the LSPR sensor. Additionally, graphene might also delay the oxidation process of the AgNPs effectively to keep the stability of the LSPR sensor, and the developed LSPR sensor exhibited good sensitivity and linearity in the detection of the ethanol and

glucose solutions. The work shows that the developed LSPR sensor may have promising applications in biosensing.

Acknowledgments

The authors are grateful for financial support from the National Natural Science Foundation of China (11674199, 11474187 and 61307120), Shandong Province Natural Science Foundation (ZR2016AM19), project funded by China Postdoctoral Science Foundation (2016M602716) and Excellent Young Scholars Research Fund of Shandong Normal University.

References

[1] Shao Y, Xu S, Zheng X, Wang Y and Xu W 2010 Optical fiber LSPR biosensor prepared by gold nanoparticle assembly on polyelectrolyte multilayer *Sensors* **10** 3585–96
[2] Lin Y, Zou Y, Mo Y, Guo J and Lindquist R G 2010 E-beam patterned gold nanodot arrays on optical fiber tips for localized surface plasmon resonance biochemical sensing *Sensors* **10** 9397–406
[3] Cao J, Tu M H, Sun T and Grattan K T 2013 Wavelength-based localized surface plasmon resonance optical fiber biosensor *Sensors Actuators* B **181** 611–9
[4] Ghodselahi T, Neishaboorynejad T and Arsalani S 2015 Fabrication LSPR sensor chip of Ag NPs and their biosensor application based on interparticle coupling *Appl. Surf. Sci.* **343** 194–201
[5] Lin H Y, Huang C H, Cheng G L, Chen N K and Chui H C 2012 Tapered optical fiber sensor based on localized surface plasmon resonance *Opt. Express* **20** 21693–701
[6] Sai V V R, Kundu T and Mukherji S 2009 Novel U-bent fiber optic probe for localized surface plasmon resonance based biosensor *Biosens. Bioelectron.* **24** 2804–9
[7] Tan Z, Hao X, Li X, Chen Y, Hong X and Fan P 2015 Angular characteristics of a multimode fibre surface plasmon resonance sensor under wavelength interrogation *J. Phys. D: Appl. Phys.* **49** 025401
[8] Esmaeilzadeh H, Arzi E, Légaré F and Hassani A 2013 Boundary integral method to calculate the sensitivity temperature error of microstructured fibre plasmonic sensors *J. Phys. D: Appl. Phys.* **46** 325103
[9] Jin R, Cao C Y, Hao E, Metraux G S, Schatz G C and Mirkin C A 2003 Controlling anisotropic nanoparticle growth through plasmon excitation *Nature* **425** 487–90
[10] Murray W, Suckling J and Barnes W 2006 Overlayers on silver nanotriangles: field confinement and spectral position of localized surface plasmon resonances *Nano Lett.* **6** 1772–7
[11] Al-Qazwini Y, Noor A S M, Al-Qazwini Z, Yaacob M H, Harun S W and Mahdi M A 2016 Refractive index sensor based on SPR in symmetrically etched plastic optical fibers *Sensors Actuators* A **246** 163–9
[12] Sepúlveda B, Angelomé P C, Lechuga L M and Liz-Marzán L M 2009 LSPR-based nanobiosensors *Nano Today* **4** 244–51
[13] Endo T, Takizawa H, Imai Y, Yanagida Y and Hatsuzawa T 2011 Study of electrical field distribution of gold-capped nanoparticle for excitation of localized surface plasmon resonance *Appl. Surf. Sci.* **257** 2560–6
[14] Ghodselahi T, Hoornam S, Vesaghi M A, Ranjbar B, Azizi A and Mobasheri H 2014 Fabrication localized surface plasmon resonance sensor chip of gold nanoparticles and detection lipase–osmolytes interaction *Appl. Surf. Sci.* **314** 138–44
[15] Sharma A K, Jha R and Gupta B 2007 Fiber-optic sensors based on surface plasmon resonance: a comprehensive review *IEEE Sens. J.* **7** 1118–29
[16] Shukla S, Sharma N K and Sajal V 2015 Sensitivity enhancement of a surface plasmon resonance based fiber optic sensor using ZnO thin film: a theoretical study *Sensors Actuators* B **206** 463–70
[17] Al-Qazwini Y, Noor A S M, Yaacob M H, Harun S W and Mahdi M A 2015 Experimental realization and performance evaluation of refractive index SPR sensor based on unmasked short tapered multimode-fiber operating in aqueous environments *Sensors Actuators* A **236** 38–43
[18] Cennamo N, D'Agostino G, Donà A, Dacarro G, Pallavicini P, Pesavento M and Zeni L 2013 Localized surface plasmon resonance with five-branched gold nanostars in a plastic optical fiber for bio-chemical sensor implementation *Sensors* **13** 14676–86
[19] Kumar S, Sharma G and Singh V 2014 Sensitivity of tapered optical fiber surface plasmon resonance sensors *Opt. Fiber Technol.* **20** 333–5
[20] Cennamo N, D'Agostino G, Pesavento M and Zeni L 2014 High selectivity and sensitivity sensor based on MIP and SPR in tapered plastic optical fibers for the detection of L-nicotine *Sensors Actuators* B **191** 529–36
[21] Ribaut C, Voisin V, Malachovská V, Dubois V, Mégret P, Wattiez R and Caucheteur C 2016 Small biomolecule immunosensing with plasmonic optical fiber grating sensor *Biosens. Bioelectron.* **77** 315–22
[22] Liang G, Zhao Z, Wei Y, Liu K, Hou W and Duan Y 2015 Plasma enhanced label-free immunoassay for alpha-fetoprotein based on a U-bend fiber-optic LSPR biosensor *RSC Adv.* **5** 23990–8
[23] Gao S S *et al* 2016 Absorbance response of a graphene oxide coated U-bent optical fiber sensor for aqueous ethanol detection *RSC Adv.* **6** 15808
[24] Bilro L, Alberto R, Pinto J L and Nogueira R 2012 Optical sensors based on plastic fibers *Sensors* **12** 12184–207
[25] Peters K 2011 Polymer optical fiber sensors—a review *Smart Mater. Struct.* **20** 013002
[26] Liz-marzan L M 2006 Tailoring surface plasmons through the morphology and assembly of metal nanoparticles *Langmuir* **22** 32–41
[27] Novoselov K S A, Geim A K, Morozov S V, Jiang D, Zhang Y, Dubonos S V, Grigorieva I V and Firsov A A 2004 Two-dimensional gas of massless Dirac fermions in graphene *Science* **306** 666–9
[28] Zhang C, Jiang S Z, Huo Y Y, Liu A H, Xu S C, Liu X Y, Sun Z C, Xu Y Y, Li Z and Man B Y 2015 SERS detection of R6G based on a novel graphene oxide/silver nanoparticles/silicon pyramid arrays structure *Opt. Express* **23** 24811–21
[29] Zhang C, Man B Y, Yang C, Jiang S Z, Liu M, Chen C S, Xu S C, Sun Z C, Gao X G and Chen X J 2013 Facile synthesis of graphene on dielectric surfaces using a two-temperature reactor CVD system *Nanotechnology* **24** 395603
[30] Elias D C *et al* 2011 Dirac cones reshaped by interaction effects in suspended graphene *Nat. Phys.* **7** 701–4
[31] Hoggard A, Wang L Y, Ma L, Fang Y, You G, Olson J, Liu Z, Chang W S, Ajayan P M and Link S 2013 Using the plasmon linewidth to calculate the time and efficiency of electron transfer between gold nanorods and graphene *ACS Nano* **7** 11209–17
[32] Kim J, Son H, Cho D J, Geng B, Regan W, Shi S, Kim K, Zettl A, Shen Y R and Wang F 2012 Electrical control of optical plasmon resonance with graphene *Nano Lett.* **12** 5598–602

[33] Niu J, Shin Y J, Lee Y, Ahn J H and Yang H 2012 Graphene induced tunability of the surface plasmon resonance *Appl. Phys. Lett.* **100** 061116
[34] Lee S, Lee M H, Shin H J and Choi D 2013 Control of density and LSPR of Au nanoparticles on graphene *Nanotechnology* **24** 275702
[35] Reckinger N, Vlad A, Melinte S, Colomer J F and Sarrazin M 2013 Graphene-coated holey metal films: tunable molecular sensing by surface plasmon resonance *Appl. Phys. Lett.* **102** 211108
[36] Zaniewski A M, Schriver M, Lee J G, Crommie M F and Zettl A 2013 Electronic and optical properties of metal-nanoparticle filled graphene sandwiches *Appl. Phys. Lett.* **102** 023108
[37] Ding Q, Shi Y, Chen M, Li H, Yang X, Qu Y, Liang W and Sun M 2016 Ultrafast dynamics of plasmon-exciton interaction of Ag nanowire-graphene hybrids for surface catalytic reactions *Sci. Rep.* **6** 32724
[38] Zhao J, Sun M, Liu Z, Quan B, Gu C and Li J 2015 Three dimensional hybrids of vertical graphene-nanosheet sandwiched by Ag-nanoparticles for enhanced surface selectively catalytic reactions *Sci. Rep.* **5** 16019
[39] Xu S, Jiang S, Wang J, Wei J, Yue W and Ma Y 2016 Graphene isolated Au nanoparticle arrays with high reproducibility for high-performance surface-enhanced Raman scattering *Sensors Actuators* B **222** 1175–83
[40] Maharana P K, Srivastava T and Jha R 2014 Low index dielectric mediated surface plasmon resonance sensor based on graphene for near infrared measurements *J. Phys. D: Appl. Phys.* **47** 385102
[41] Bhatia P, Yadav P and Gupta B D 2013 Surface plasmon resonance based fiber optic hydrogen peroxide sensor using polymer embedded nanoparticles *Sensors Actuators* B **182** 330–5
[42] Vineeshkumar T V, Rithesh Raj D, Prasanth S, Unnikrishnan N V, Philip R and Sudarsanakumar C 2014 Structural and optical studies of $Zn_{1-x}Cd_xS$ quantum dots synthesized by *in situ* technique in PVA matrix *Opt. Mater.* **37** 439–45
[43] Ortega-Mendoza J G, Padilla-Vivanco A, Toxqui-Quitl C, Zaca-Morán P, Villegas-Hernández D and Chávez F 2014 Optical fiber sensor based on localized surface plasmon resonance using silver nanoparticles photodeposited on the optical fiber end *Sensors* **14** 18701–10
[44] Srivastava S K, Arora V, Sapra S and Gupta B D 2012 Localized surface plasmon resonance-based fiber optic U-shaped biosensor for the detection of blood glucose *Plasmonics* **7** 261–8
[45] Khijwania S K and Gupta B D 2000 Maximum achievable sensitivity of the fiber optic evanescent field absorption sensor based on the U-shaped probe *Opt. Commun.* **175** 135–7